Dalton Transactions

ROYAL SOCIETY OF CHEMISTRY

PAPER

View Article Online
View Journal | View Issue

Cite this: *Dalton Trans.*, 2025, **54**, 8234

Ligand-directed top-down synthesis of trivacant lacunary polyoxomolybdates from plenary Keggin-type $[\alpha\text{-}XMo_{12}O_{40}]^{3-}$ (X = P, As, V) in organic media†

Atsuhiro Jimbo, Chifeng Li, Kentaro Yonesato, Kazuya Yamaguchi and Kosuke Suzuki *

Lacunary polyoxometalates (POMs), featuring highly reactive vacant sites, serve as valuable building blocks and precursors for the rational design of functional materials with widespread applications in catalysis, analytical chemistry, energy conversion and storage, medicine, and optical materials. While diverse Keggin-type polyoxotungstates, including both plenary and lacunary species, have been synthesized through dehydration condensation reactions and equilibrium displacement in aqueous solvents, the isolation and use of lacunary polyoxomolybdates remain challenging. To address this, the current study proposes a "ligand-directed top-down synthetic approach" for producing lacunary polyoxomolybdates from plenary Keggin-type species in organic solvents. By reacting plenary Keggin-type polyoxomolybdates $[\alpha\text{-}XMo_{12}O_{40}]^{3-}$ (X = P, As, V) with 4-methoxypyridine (pyOMe) in acetonitrile, we successfully synthesized the corresponding trivacant lacunary polyoxomolybdates ($[XMo_9O_{31}(pyOMe)_3]^{3-}$), where the vacant sites are stabilized by three pyOMe ligands. Remarkably, this approach enables the synthesis of a lacunary vanadomolybdate, a species previously unattainable through equilibrium control in aqueous systems. Furthermore, the reversible coordination of pyOMe ligands to molybdenum atoms at the vacant sites makes these lacunary polyoxomolybdates highly versatile precursors for assembling POM–organic hybrids. Overall, this study introduces an innovative synthetic methodology for POMs, demonstrating notable potential for advancing the development of functional materials.

Received 31st January 2025,
Accepted 24th February 2025

DOI: 10.1039/d5dt00252d

rsc.li/dalton

Introduction

Polyoxometalates (POMs), a class of precisely defined anionic metal oxide clusters (*e.g.*, W^{6+}, Mo^{6+}, and V^{5+}), have garnered considerable attention owing to their structural diversity and remarkable physicochemical properties.[1,2] These clusters are highly versatile, with widespread applications in catalysis, analytical chemistry, energy conversion and storage, medicine, and optical materials. This versatility stems from their tunable properties, including redox potentials, acidity, and stability, which can be finely adjusted by modifying their structures, constituent elements, and oxidation states. Among the various types of POMs, Keggin-type POMs $[XM_{12}O_{40}]^{n-}$ stand out for their ability to exhibit diverse properties depending on their central heteroatoms (X; *e.g.*, P^{5+}, As^{5+}, Si^{4+}, Ge^{4+}) and polyatoms (M; *e.g.*, W^{6+}, Mo^{6+}). These compounds are typically synthesized through dehydration condensation and equilibrium displacement in aqueous solvents, with careful control over pH conditions, metal ion concentrations, and mixing ratios. To date, extensive research has been conducted on the equilibrium and speciation profiles of polyoxotungstates in aqueous solvents,[3] enabling the isolation of fully occupied plenary $[XW_{12}O_{40}]^{n-}$ species, along with various lacunary species including monovacant $[XW_{11}O_{39}]^{n-}$, divacant $[XW_{10}O_{36}]^{n-}$, and trivacant $[XW_9O_{34}]^{n-}$ polyoxotungstates (*e.g.*, X = P^{5+}, As^{5+}, Si^{4+}, Ge^{4+}) (Fig. 1a).[4] These lacunary polyoxotungstates, with reactive vacant sites, serve as valuable building blocks and precursors for designing functional materials.[4] For instance, our group synthesized various advanced materials, such as multinuclear metal-oxo nanoclusters,[5] metal nanoclusters,[6] and organic–POM hybrids, using lacunary POMs in organic solvents.[7]

Polyoxomolybdates, another prominent class of POMs, are characterized by electrochemical, photochemical, and physico-

Department of Applied Chemistry, School of Engineering, The University of Tokyo, 7-3-1 Hongo, Bunkyo-ku, Tokyo 113-8656, Japan.
E-mail: ksuzuki@appchem.t.u-tokyo.ac.jp

†Electronic supplementary information (ESI) available: Experimental details, Tables S1–S5 and Fig. S1–S14. CCDC 2408026–2408031. For ESI and crystallographic data in CIF or other electronic format see DOI: **https://doi.org/10.1039/d5dt00252d**

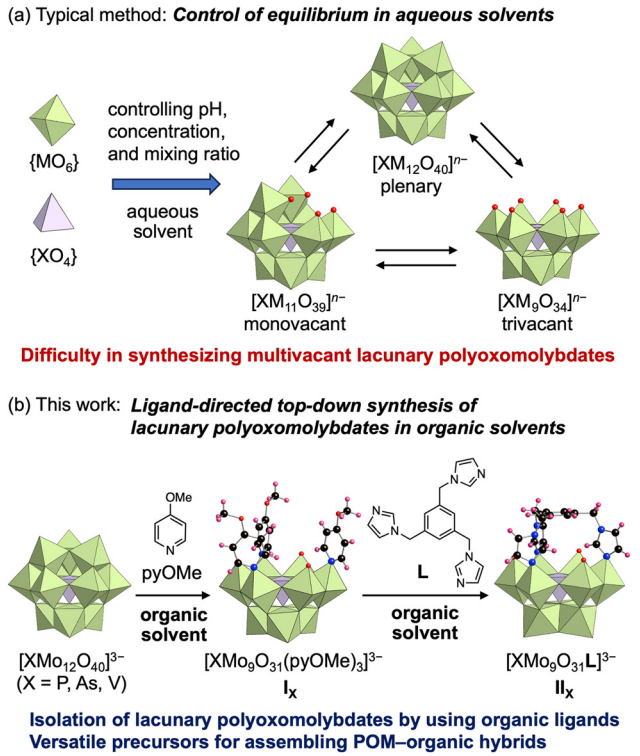

Fig. 1 (a) Typical synthesis of lacunary polyoxomolybdates *via* equilibrium control in aqueous solvents. (b) Proposed approach: ligand-directed top-down synthesis of trivacant lacunary polyoxomolybdates ($\mathbf{I_X}$, $TBA_3[XMo_9O_{31}(pyOMe)_3]$, X = P, As, V) from plenary species $[XMo_{12}O_{40}]^{3-}$ in organic solvents and their application in the synthesis of polyoxomolybdate–organic hybrids ($\mathbf{II_X}$).

chemical properties that substantially differ from those of their tungsten-based counterparts.[8] Similar to polyoxotungstates, the speciation profiles of phosphomolybdates (P/Mo),[9a,b] arsenomolybdates (As/Mo),[9c,d] and vanadomolybdates (V/Mo)[9e] in aqueous solvents have been extensively researched. Recently, computational studies have further explored the speciation profiles of phosphomolybdates[10a] and arsenomolybdates.[10b] However, achieving structural control of polyoxomolybdates through equilibrium displacement in aqueous solvents remains challenging, partly because most lacunary species exist as minor species in equilibrium mixtures (Fig. 1a). Although multivacant polyoxomolybdates are promising as building blocks for functional materials owing to the high reactivity of their vacant sites and their distinctive redox properties, the synthesis of these compounds using aqueous synthetic mixtures and their subsequent characterization remain challenging. To date, the trivacant lacunary Keggin-type phosphomolybdate $[PMo_9O_{34}]^{9-}$ is the only multivacant polyoxomolybdate that has been isolated from aqueous mixtures.[11] The use of multivacant lacunary polyoxomolybdates is further limited by their inherent structural instability. For instance, $[PMo_9O_{34}]^{9-}$ is prone to structural transformations or decomposition during reactions with metal ions or organic ligands in both aqueous and organic solvents.[12] To address these challenges, our group recently developed a method to stabilize $[PMo_9O_{34}]^{9-}$ by coordinating pyridine ligands to Mo atoms at the vacant sites in organic solvents.[13] This reversible coordination afforded a pyridine-stabilized lacunary phosphomolybdate ($[PMo_9O_{31}(py)_3]^{3-}$; py = pyridine), serving as a versatile precursor for incorporating metal ions[14] and constructing POM–organic hybrids.[13,15] Using this method, we also achieved a ligand-directed structural transformation of $[PMo_9O_{34}]^{9-}$ into a novel divacant lacunary polyoxomolybdate, $[PMo_{10}O_{34}(py)_2]^{3-}$,[15a] which has not been previously observed in aqueous POM chemistry.[3,9,10]

Building on these insights, we hypothesized that equilibrium control using organic protecting ligands in organic solvents could mitigate undesired hydrolysis, condensation, and structural decomposition. This study aimed to develop a reproducible method for synthesizing and stabilizing new lacunary polyoxomolybdates while enabling their use in functional material assembly. Accordingly, in this study, we propose a "top-down synthetic approach" for preparing lacunary Keggin-type polyoxomolybdates from their plenary precursors through ligand-directed equilibrium control in organic solvents (Fig. 1b). By reacting tetra-*n*-butylammonium (TBA) salts of plenary Keggin-type polyoxomolybdates $[\alpha\text{-}XMo_{12}O_{40}]^{3-}$ (X = P, As, V) with 4-methoxypyridine (pyOMe, C_6H_7NO) in acetonitrile, we selectively convert them into the corresponding trivacant lacunary polyoxomolybdates $\mathbf{I_X}$ ($TBA_3[XMo_9O_{31}(pyOMe)_3]$). In these products, three pyOMe ligands stabilize the structure through coordination with Mo atoms. Notably, this method enables the synthesis of lacunary vanadomolybdate $\mathbf{I_V}$, a species previously unobserved under aqueous equilibrium conditions. Furthermore, the stabilized lacunary polyoxomolybdates $\mathbf{I_X}$ serve as precursors for assembling POM–organic hybrids $\mathbf{II_X}$. Overall, this study lays the foundation for the expanded exploration and application of lacunary polyoxomolybdates in the development of functional materials, offering promising new directions in advanced POM chemistry and the design of materials for diverse applications, such as catalysis, energy conversion, and energy storage.

Results and discussion

In aqueous solutions, the equilibrium of Keggin-type POMs typically favors the formation of lacunary POMs from plenary species under high pH conditions (*i.e.*, high hydroxide concentrations).[3] Inspired by this, we explored the synthesis of lacunary polyoxomolybdates in organic solvents, beginning with the reaction of $TBA_3[\alpha\text{-}PMo_{12}O_{40}]$ (**PMo12**) with TBAOH as a base in acetonitrile at room temperature (~25 °C). Specifically, two different molar equivalents of TBAOH (1 or 10 equivalents relative to **PMo12**) were investigated. When treated with 1 equivalent of TBAOH, **PMo12** retained its original structure, as confirmed by both phosphorus-31 nuclear magnetic resonance (^{31}P NMR) spectroscopy and electrospray ionization mass (ESI-mass) spectrometry (Fig. 2a and e). However, upon adding 10 equivalents of TBAOH, the ^{31}P NMR spectrum of the reaction

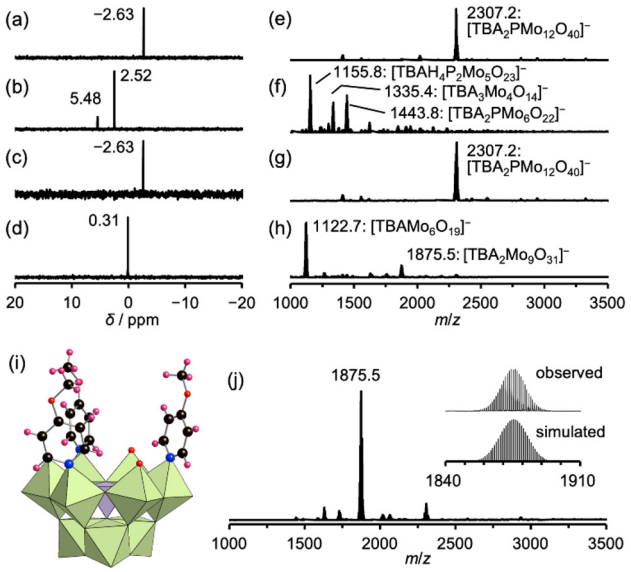

Fig. 2 (a–d) ^{31}P NMR and (e–h) ESI-mass spectra of the reaction mixtures used for synthesizing lacunary POMs from **PMo12** in acetonitrile under various conditions: (a and e) **PMo12** after reacting with 1 equivalent of TBAOH for 1 h; (b and f) **PMo12** after reacting with 10 equivalents of TBAOH for 1 h; (c and g) **PMo12** after reacting with 250 equivalents of pyridine for 1 h; and (d and h) **PMo12** after reacting with 250 equivalents of pyOMe for 15 min. (i) Crystal structure of the anionic component of $\mathbf{I_P}$. (j) ESI-mass spectrum of $\mathbf{I_P}$ in acetonitrile. Inset: enlarged spectrum (top) and simulated pattern of $[TBA_2PMo_9O_{31}]^-$ (*m*/*z*: 1875.5, bottom). Light green octahedra and the light purple tetrahedron represent $[MoO_6]$ and $[PO_4]$, respectively. Red, black, pink, and blue spheres denote O, C, H, and N atoms, respectively.

mixture displayed peaks at 2.52 ppm (major species) and 5.48 ppm (minor species) (Fig. 2b). Correspondingly, the ESI-mass spectrum of the mixture revealed the formation of decomposed species, identified as $[P_2Mo_5O_{23}]^{6-}$ (*m*/*z* = 1155.8, $[TBAH_4P_2Mo_5O_{23}]^-$) and $[PMo_6O_{22}]^{3-}$ (*m*/*z* = 1443.8, $[TBA_2PMo_6O_{22}]^-$) (Fig. 2f). These species likely correspond to the 2.52 and 5.48 ppm signals observed in the ^{31}P NMR spectrum.[9a,16] Thus, the reaction between **PMo12** and TBAOH did not yield the desired lacunary polyoxomolybdates but instead resulted in decomposition. To overcome this issue, we tested the addition of pyridine, intended to act as both a base and a stabilizing ligand for lacunary polyoxomolybdates. However, treating **PMo12** with 250 equivalents of pyridine in acetonitrile for 1 h produced no observable structural changes in **PMo12**, as evidenced by its ^{31}P NMR and ESI-mass spectra (Fig. 2c and g).

Consequently, to facilitate the structural transformation, 4-methoxypyridine (pyOMe, C_6H_7NO; pK_a = 14.23 in acetonitrile), a ligand with higher basicity than pyridine (pK_a = 12.53 in acetonitrile), was used.[17] When **PMo12** was reacted with 250 equivalents of pyOMe at room temperature (~25 °C) for 15 min, the peak corresponding to **PMo12** disappeared from the ^{31}P NMR spectrum, while a new peak appeared at 0.31 ppm, indicating the structural transformation of **PMo12** into a new species (Fig. 2d). The ESI-mass spectrum confirmed the formation of a trivacant lacunary structure, with a prominent set of signals centered at *m*/*z* = 1875.5, attributed to $[TBA_2PMo_9O_{31}]^-$ (theoretical *m*/*z*: 1875.5) (Fig. 2h). The ESI-mass spectrum displayed another set of signals centered at *m*/*z* = 1122.7, attributed to $[TBAMo_6O_{19}]^-$, confirming the formation of a byproduct, $[Mo_6O_{19}]^{2-}$ (*i.e.*, the Lindqvist-type cluster).

Crystallizing the reaction mixture by adding diethyl ether yielded single crystals suitable for X-ray diffraction analysis. This analysis revealed that the anionic component of the product ($\mathbf{I_P}$) was a trivacant lacunary A-α-Keggin-type phosphomolybdate, $[A\text{-}\alpha\text{-}PMo_9O_{31}(pyOMe)_3]^{3-}$, featuring three pyOMe molecules coordinated to Mo atoms at the vacant sites (Fig. 2i and Table S1†). Notably, the ESI-mass spectrum of the $\mathbf{I_P}$ crystals in acetonitrile displayed a set of signals centered at *m*/*z* = 1875.5, attributed to $[TBA_2PMo_9O_{31}]^-$; however, no signals corresponding to $[Mo_6O_{19}]^{2-}$ were apparent (Fig. 2j). The ESI-mass spectrum also suggested the dissociation of pyOMe ligands from the Mo atoms during the ionization process, which occurred during the ESI-mass spectrometry analysis. Further, elemental analysis confirmed that $[Mo_6O_{19}]^{2-}$ did not crystallize, resulting in the high-purity isolation of $\mathbf{I_P}$. Comprehensive characterization using various techniques—including X-ray crystallography, ESI-mass spectrometry, thermogravimetric (TG) analysis (Fig. S1†), and elemental analysis—validated the molecular formula of $\mathbf{I_P}$ as $TBA_3[A\text{-}\alpha\text{-}PMo_9O_{31}(pyOMe)_3]\cdot 3(H_2O)$. These findings indicate that $\mathbf{I_P}$ was synthesized *via* a top-down transformation of plenary **PMo12** in the presence of a base and protective pyOMe ligands, yielding $[Mo_6O_{19}]^{2-}$ as a byproduct. This transformation is represented by the following reaction equation: $[\alpha\text{-}PMo_{12}O_{40}]^{3-} + OH^- + 3pyOMe \rightarrow [A\text{-}\alpha\text{-}PMo_9O_{31}(pyOMe)_3]^{3-} + 0.5[Mo_6O_{19}]^{2-} + 0.5H_2O$. Density functional theory (DFT) calculations further supported the thermodynamic feasibility of this reaction, with a standard Gibbs energy change of the reaction ($\Delta_rG°$) of −51.02 kJ mol^{-1} (equilibrium constant, $K = 8.77 \times 10^8$ at 298 K).

The reaction of **PMo12** with 250 equivalents of 4-cyanopyridine (pyCN, $C_6H_4N_2$; pK_a = 8.50 in acetonitrile), a ligand with lower basicity than pyridine (pK_a = 12.53 in acetonitrile),[17,18] in acetonitrile did not induce any structural transformation in **PMo12** (Fig. S2†). However, when $\mathbf{I_P}$ was reacted with 250 equivalents of pyCN in acetonitrile for 1 h, followed by crystallization using diethyl ether, single crystals of **PMo9-pyCN** were obtained. X-ray crystallographic analysis revealed that **PMo9-pyCN** was structurally analogous to $\mathbf{I_P}$, featuring three pyCN molecules coordinated to the Mo atoms at the vacant sites of the trivacant A-α-Keggin-type $\{PMo_9\}$ structure (Fig. S3 and Table S2†). Based on the results of X-ray crystallography, ESI-mass spectrometry (Fig. S4†), TG analysis (Fig. S5†), and elemental analysis, the molecular formula for **PMo9-pyCN** was determined to be $TBA_3[A\text{-}\alpha\text{-}PMo_9O_{31}(pyCN)_3]$. Notably, **PMo9-pyCN** could not be synthesized directly from **PMo12** *via* the proposed direct top-down approach using pyCN, likely owing to the ligand's low basicity and weak coordination ability. Instead, it was successfully afforded through a ligand exchange

reaction with $\mathbf{I_P}$, as indicated by the following equation: $[A\text{-}\alpha\text{-}PMo_9O_{31}(pyOMe)_3]^{3-}$ + 3pyCN → $[A\text{-}\alpha\text{-}PMo_9O_{31}(pyCN)_3]^{3-}$ + 3pyOMe. These results highlight the critical role of both ligand basicity and coordination ability in the ligand-directed synthesis of lacunary species derived from **PMo12**. To further examine this dependency, a combined approach employing pyridine and an additional base was explored. When **PMo12** was reacted with 250 equivalents of pyridine and 2 equivalents of TBAOH in acetonitrile at room temperature (~25 °C) for 1 h, the ^{31}P NMR and ESI-mass spectra confirmed the conversion of **PMo12** into $\mathbf{I_P}$. These observations showed that the combination of a ligand and a base effectively facilitates the structural transformation of **PMo12** (Fig. S6†).

To extend this ligand-directed synthesis methodology to arsenomolybdate, we examined **AsMo12** ($TBA_3[\alpha\text{-}AsMo_{12}O_{40}]$), a compound structurally analogous to **PMo12** with heteroatom substitution. While previous studies examining the speciation profiles of arsenomolybdates in aqueous solvents have suggested the potential formation of a trivacant lacunary species,[9c,d,10b] successful isolation of this species is yet to be reported. When **AsMo12** was reacted with 250 equivalents of pyOMe in acetonitrile at room temperature (~25 °C) for 1 h, the ESI-mass spectrum of the reaction solution displayed a set of signals centered at m/z = 1919.5, attributed to $[TBA_2AsMo_9O_{31}]^-$, indicating the formation of a trivacant lacunary species (Fig. S7†). This ESI-mass spectrum also revealed the formation of $[Mo_6O_{19}]^{2-}$ (m/z = 1122.6) as a byproduct. Further, crystallization of the reaction mixture using p-xylene yielded single crystals of $\mathbf{I_{As}}$. X-ray crystallographic analysis confirmed that the anionic structure of $\mathbf{I_{As}}$ closely resembled that of $\mathbf{I_P}$, with a trivacant lacunary configuration stabilized by three pyOMe ligands (Fig. 3a and Table S3†). The ESI-mass spectrum of $\mathbf{I_{As}}$ crystals in acetonitrile displayed a set of signals centered at m/z = 1919.5, attributed to $[TBA_2AsMo_9O_{31}]^-$; however, no signals corresponding to $[Mo_6O_{19}]^{2-}$ were apparent (Fig. 3b). Combined with the elemental analysis outcomes, these results demonstrate the exclusion of the byproduct ($[Mo_6O_{19}]^{2-}$) during crystallization, ensuring the high purity of $\mathbf{I_{As}}$. Comprehensive characterization through several techniques, including X-ray crystallography, ESI-mass spectrometry, TG analysis (Fig. S8†), and elemental analysis, confirmed the molecular formula of $\mathbf{I_{As}}$ as $TBA_3[A\text{-}\alpha\text{-}AsMo_9O_{31}(pyOMe)_3]\cdot 2(CH_3CN)$. The formation of $\mathbf{I_{As}}$ likely followed a reaction mechanism similar to that of $\mathbf{I_P}$: $[\alpha\text{-}AsMo_{12}O_{40}]^{3-}$ + OH^- + 3pyOMe → $[A\text{-}\alpha\text{-}AsMo_9O_{31}(pyOMe)_3]^{3-}$ + $0.5[Mo_6O_{19}]^{2-}$ + $0.5H_2O$. DFT calculations again confirmed the thermodynamic feasibility of this reaction, yielding a $\Delta_rG°$ value of −76.78 kJ mol^{-1} ($K = 2.87 \times 10^{13}$ at 298 K).

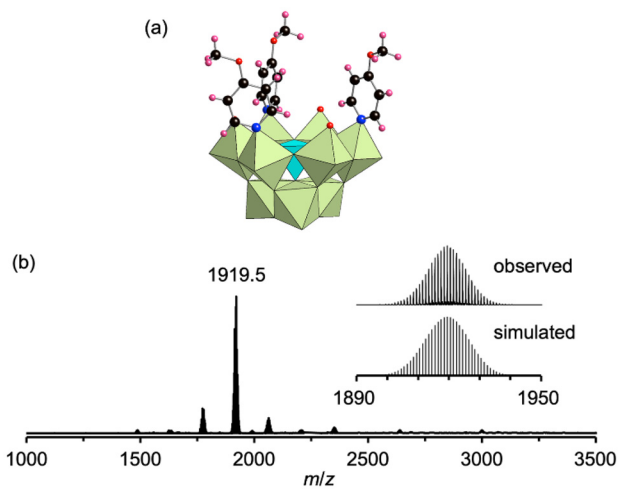

Fig. 3 (a) Crystal structure of the anionic component of $\mathbf{I_{As}}$. (b) ESI-mass spectrum of $\mathbf{I_{As}}$ in acetonitrile. Inset: enlarged spectrum (top) and simulated pattern of $[TBA_2AsMo_9O_{31}]^-$ (m/z: 1919.5, bottom). Light green octahedra and the light blue tetrahedron represent $[MoO_6]$ and $[AsO_4]$, respectively. Red, black, pink, and blue spheres denote O, C, H, and N atoms, respectively.

Building on these findings, we sought to synthesize previously unreported lacunary structures, focusing on vanadomolybdates containing a pentavalent heteroatom (V^{5+}), analogous to phosphomolybdates (P^{5+}) and arsenomolybdates (As^{5+}). Notably, lacunary vanadomolybdate species are yet to be identified in speciation studies using aqueous solvents.[9e] Previous reports in this context have been limited to the synthesis of a lacunary vanadoxomolybdate capped by a triol at Mo atoms lying opposite the vacant site.[19] To investigate the formation of lacunary vanadomolybdates, $TBA_3[\alpha\text{-}VMo_{12}O_{40}]$ (**VMo12**) was reacted with 250 equivalents of pyOMe in acetonitrile at room temperature (~25 °C) for 1 h. The ESI-mass spectrum of the reaction mixture displayed a set of signals centered at m/z = 1895.5, attributed to $[TBA_2VMo_9O_{31}]^-$, confirming the successful formation of a trivacant species. The spectrum also indicated the formation of $[Mo_6O_{19}]^{2-}$ (m/z = 1122.6) as a byproduct (Fig. S9†). Crystallization using mesitylene as a precipitant yielded single crystals of $\mathbf{I_V}$. X-ray crystallographic analysis revealed that $\mathbf{I_V}$ adopted a trivacant lacunary Keggin-type vanadomolybdate structure stabilized by three pyOMe ligands coordinated to Mo atoms at the vacant sites (Fig. 4 and Table S4†). Intriguingly, some $\{VMo_9\}$ units transformed from an α-type structure to a β-type structure *via* an approximately 60° rotation of the $[Mo_3O_{13}]$ unit, yielding an α/β ratio of 0.75 : 0.25, as confirmed by X-ray crystallography and ^{51}V NMR spectroscopy (Fig. S10†). The ESI-mass spectrum of $\mathbf{I_V}$ crystals in acetonitrile displayed a set of signals centered at m/z = 1895.6, attributed to $[TBA_2VMo_9O_{31}]^-$, with no detectable presence of $[Mo_6O_{19}]^{2-}$. This confirmed the effective exclusion of the byproduct from crystallization (Fig. 4b). Combining the results of X-ray crystallography, ESI-mass spectrometry, TG analysis (Fig. S11†), and elemental analysis, the molecular formula of $\mathbf{I_V}$ was determined to be $TBA_3[VMo_9O_{31}(pyOMe)_3]\cdot 3(H_2O)\cdot 0.5(CH_3CN)$. DFT calculations further revealed $\Delta_rG°$ values of −94.43 and −89.70 kJ mol^{-1} for the transformation of $TBA_3[\alpha\text{-}VMo_{12}O_{40}]$ into the α- and β-type structures of $\mathbf{I_V}$, respectively, demonstrating that the α-type structure is thermodynamically more favorable.

Finally, we explored the potential of the $\mathbf{I_X}$ species as precursors for the synthesis of functional materials. Leveraging the reversible coordination of pyOMe ligands with the Mo

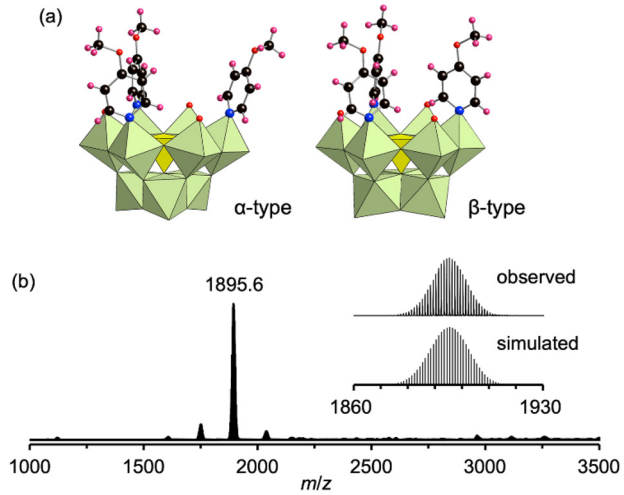

Fig. 4 (a) Crystal structure of the anionic component of $\mathbf{I_V}$: α-type (left) and β-type (right). (b) ESI-mass spectrum of $\mathbf{I_V}$ in acetonitrile. Inset: enlarged spectrum (top) and simulated pattern of $[TBA_2VMo_9O_{31}]^-$ (*m*/*z*: 1895.5, bottom). Light green octahedra and the yellow tetrahedron represent $[MoO_6]$ and $[VO_4]$, respectively. Red, black, pink, and blue spheres denote O, C, H, and N atoms, respectively.

atoms at the vacant sites, we investigated their reactivity with imidazole ligands, which effectively coordinate with lacunary polyoxomolybdates, as demonstrated in our recent study.[15c] The reaction of $\mathbf{I_V}$ with 2 equivalents of 1,3,5-tris[(1*H*-imidazol-1-yl)methyl]benzene (**L**, $C_{18}H_{18}N_6$, Fig. 1b) in acetonitrile at 80 °C for 30 min, followed by the addition of mesitylene, afforded single crystals of $\mathbf{II_V}$. X-ray crystallographic analysis revealed that the anionic structure of $\mathbf{II_V}$ adopted a capped monomeric configuration, comprising a $\{VMo_9\}$ unit and a single **L** ligand coordinated to three Mo atoms at the vacant site (Fig. 5a and Table S5†). Interestingly, X-ray crystallography analysis revealed that $\mathbf{II_V}$ contained a mixture of α- and β-type $\{VMo_9\}$ units, with an α/β ratio of 0.20 : 0.80. This indicates that some α-type $\{VMo_9\}$ units from $\mathbf{I_V}$ (α/β ratio of 0.75 : 0.25) transformed into β-type units. The ESI-mass spectrum of $\mathbf{II_V}$ in acetonitrile displayed a set of signals centered at *m*/*z* = 2457.0 and 2698.2, attributed to $[TBA_3HVMo_9O_{31}\mathbf{L}]^+$ and $[TBA_4VMo_9O_{31}\mathbf{L}]^+$, respectively, confirming that the POM–organic hybrid structure was retained in the solution phase (Fig. 5b). Similarly, the reaction of $\mathbf{I_{As}}$ with ligand **L** afforded $\mathbf{II_{As}}$, a structural analogue of $\mathbf{II_V}$, comprising α- and β-type $\{AsMo_9\}$ units with an α/β ratio of 0.08 : 0.92 (Fig. S12a and Table S5†). Further, the ESI-mass spectrum of $\mathbf{II_{As}}$ in acetonitrile presented a set of signals centered at *m*/*z* = 2480.9 and 2723.2, attributed to $[TBA_3HAsMo_9O_{31}\mathbf{L}]^+$ and $[TBA_4AsMo_9O_{31}\mathbf{L}]^+$, respectively (Fig. S12b†). These results confirm the first successful synthesis of POM–organic hybrids using trivacant lacunary vanadomolybdate and arsenomolybdate as precursors.

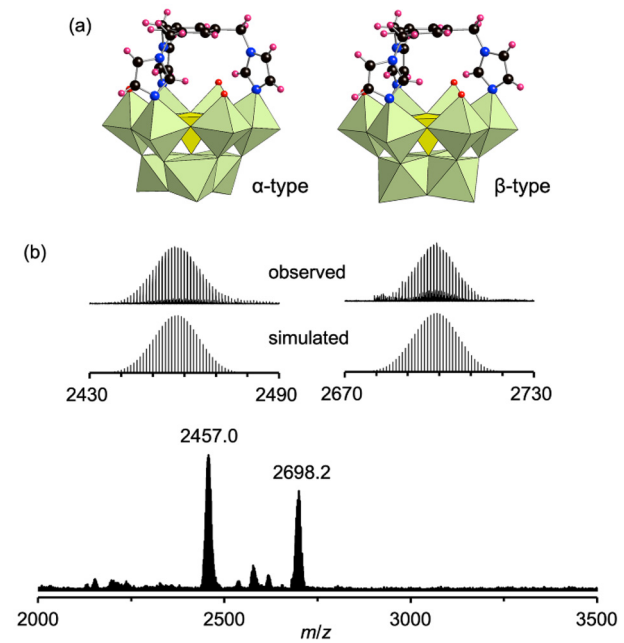

Fig. 5 (a) Crystal structure of the anionic component of $\mathbf{II_V}$: α-type (left) and β-type (right). (b) ESI-mass spectrum of $\mathbf{II_V}$ in acetonitrile. Inset: enlarged spectrum (top) and simulated pattern of $[TBA_3HVMo_9O_{31}\mathbf{L}]^+$ (*m*/*z*: 2457.0, bottom) and $[TBA_4VMo_9O_{31}\mathbf{L}]^+$ (*m*/*z*: 2698.2, bottom) (**L** = $C_{18}H_{18}N_6$). Light green octahedra and the yellow tetrahedron represent $[MoO_6]$ and $[VO_4]$, respectively. Red, black, pink, and blue spheres denote O, C, H, and N atoms, respectively.

Conclusions

In conclusion, we successfully developed a novel ligand-directed top-down synthetic approach for producing trivacant lacunary Keggin-type polyoxomolybdates $\mathbf{I_X}$ ($TBA_3[XMo_9O_{31}(pyOMe)_3]$, X = P, As, V) from their plenary counterparts $TBA_3[XMo_{12}O_{40}]$ using 4-methoxypyridine (pyOMe) as a protecting ligand in organic solvents. Our investigations using alternative pyridine ligands highlighted the critical roles of ligand basicity and coordination ability in driving this synthesis. Notably, the proposed approach enabled the synthesis of a new trivacant lacunary vanadomolybdate, a species not previously observed in aqueous systems. Furthermore, pyOMe-protected $\mathbf{I_X}$ species were successfully transformed into POM–organic hybrids $\mathbf{II_X}$ through reactions with a multidentate imidazole-based ligand (**L**), demonstrating their versatility as precursors. The proposed ligand-directed synthetic strategy provides access to previously unexplored lacunary POMs and opens new pathways for the development of diverse functional materials leveraging these lacunary POMs as building blocks.

Data availability

The data supporting this manuscript is available in the ESI† of and available on request. Crystallographic data for $\mathbf{I_P}$, **PMo9-pyCN**, $\mathbf{I_{As}}$, $\mathbf{I_V}$, $\mathbf{II_{As}}$, and $\mathbf{II_V}$ have been deposited at the CCDC (deposition numbers 2408026–2408031).†

Conflicts of interest

There are no conflicts to declare.

Acknowledgements

This study was supported in part by JST FOREST (JPMJFR213M), JSPS KAKENHI (24K01448, 22H04971), and the JSPS Core-to-Core program. A part of computations was performed using Research Center for Computational Science, Okazaki, Japan (Project: 23-IMS-C106, 24-IMS-C101).

References

1 (*a*) M. T. Pope, *Heteropoly and Isopoly Oxometalates*, Springer, Berlin, 1983; (*b*) C. L. Hill, in *Comprehensive Coordination Chemistry II*, ed. J. A. McCleverty and T. J. Meyer, Elsevier Pergamon, Amsterdam, 2004, vol. 4, p. 6792.

2 (*a*) M. Sadakane and E. Steckhan, *Chem. Rev.*, 1998, **98**, 219; (*b*) A. Misra, K. Kozma, C. Streb and M. Nyman, *Angew. Chem., Int. Ed.*, 2020, **59**, 596; (*c*) U. Kortz, A. Müller, J. Van Slageren, J. Schnack, N. S. Dalal and M. Dressel, *Coord. Chem. Rev.*, 2009, **253**, 2315; (*d*) H. Lv, Y. V. Geletii, C. Zhao, J. W. Vickers, G. Zhu, Z. Luo, J. Song, T. Lian, D. G. Musaev and C. L. Hill, *Chem. Soc. Rev.*, 2012, **41**, 7572; (*e*) H. N. Miras, J. Yan, D.-L. Long and L. Cronin, *Chem. Soc. Rev.*, 2012, **41**, 7403; (*f*) M. Nyman and P. C. Burns, *Chem. Soc. Rev.*, 2012, **41**, 7354; (*g*) I. A. Weinstock, R. E. Schreiber and R. Neumann, *Chem. Rev.*, 2018, **118**, 2680; (*h*) N. I. Gumerova and A. Rompel, *Nat. Rev. Chem.*, 2018, **2**, 0112; (*i*) M. Lechner, R. Güttel and C. Streb, *Dalton Trans.*, 2016, **45**, 16716; (*j*) K. Suzuki, N. Mizuno and K. Yamaguchi, *ACS Catal.*, 2018, **8**, 10809; (*k*) S. Uchida, *Chem. Sci.*, 2019, **10**, 7670.

3 (*a*) N. I. Gumerova and A. Rompel, *Chem. Soc. Rev.*, 2020, **49**, 7568; (*b*) N. I. Gumerova and A. Rompel, *Sci. Adv.*, 2023, **9**, eadi0814; (*c*) E. Petrus, D. Garay-Ruiz, M. Reiher and C. Bo, *J. Am. Chem. Soc.*, 2023, **145**, 18920.

4 (*a*) O. Oms, A. Dolbecq and P. Mialane, *Chem. Soc. Rev.*, 2012, **41**, 7497; (*b*) S.-T. Zheng and G.-Y. Yang, *Chem. Soc. Rev.*, 2012, **41**, 7623; (*c*) J. M. Cameron, G. Guillemot, T. Galambos, S. S. Amin, E. Hampson, K. M. Haidaraly, G. N. Newton and G. Izzet, *Chem. Soc. Rev.*, 2022, **51**, 293; (*d*) L.-L. Liu, L. Wang, X.-Y. Xiao, P. Yang, J. Zhao and U. Kortz, *Coord. Chem. Rev.*, 2024, **506**, 215687.

5 (*a*) K. Suzuki, N. Mizuno and K. Yamaguchi, *J. Jpn. Pet. Inst.*, 2020, **63**, 258; (*b*) K. Suzuki, F. Tang, Y. Kikukawa, K. Yamaguchi and N. Mizuno, *Angew. Chem., Int. Ed.*, 2014, **53**, 5356; (*c*) T. Minato, D. Salley, N. Mizuno, K. Yamaguchi, L. Cronin and K. Suzuki, *J. Am. Chem. Soc.*, 2021, **143**, 12809; (*d*) K. Sato, K. Yonesato, T. Yatabe, K. Yamaguchi and K. Suzuki, *Chem. – Eur. J.*, 2022, **28**, e202104051.

6 (*a*) K. Yonesato, H. Ito, H. Itakura, D. Yokogawa, T. Kikuchi, N. Mizuno, K. Yamaguchi and K. Suzuki, *J. Am. Chem. Soc.*, 2019, **141**, 19550; (*b*) K. Yonesato, D. Yanai, S. Yamazoe, D. Yokogawa, T. Kikuchi, K. Yamaguchi and K. Suzuki, *Nat. Chem.*, 2023, **15**, 940; (*c*) Y. Koizumi, K. Yonesato, S. Kikkawa, S. Yamazoe, K. Yamaguchi and K. Suzuki, *J. Am. Chem. Soc.*, 2024, **146**, 14610.

7 M. Yamgauchi, K. Shioya, C. Li, K. Yonesato, K. Murata, K. Ishii, K. Yamaguchi and K. Suzuki, *J. Am. Chem. Soc.*, 2024, **146**, 4549.

8 (*a*) A. M. Khenkin, G. Leitus and R. Neumann, *J. Am. Chem. Soc.*, 2010, **132**, 11446; (*b*) B. Nohra, H. E. Moll, L. M. R. Albelo, P. Mialane, J. Marrot, C. Mellot-Draznieks, M. O'Keeffe, R. N. Biboum, J. Lemaire, B. Keita, L. Nadjo and A. Dolbecq, *J. Am. Chem. Soc.*, 2011, **133**, 13363; (*c*) J.-S. Qin, D.-Y. Du, W. Guan, X.-J. Bo, Y.-F. Li, L.-P. Guo, Z.-M. Su, Y.-Y. Wang, Y.-Q. Lan and H.-C. Zhou, *J. Am. Chem. Soc.*, 2015, **137**, 7169; (*d*) J. Lehmann, A. Gaita-Arino, E. Coronado and D. Loss, *Nat. Nanotechnol.*, 2007, **2**, 312; (*e*) V. Prabhakaran, B. L. Mehdi, J. J. Ditto, M. H. Engelhard, B. Wang, K. D. D. Gunaratne, D. C. Johnson, N. D. Browning, G. E. Johnson and J. Laskin, *Nat. Commun.*, 2016, **7**, 11399; (*f*) N. Kawasaki, H. Wang, R. Nakanishi, S. Hamanaka, R. Kitaura, H. Shinohara, T. Yokoyama, H. Yoshikawa and K. Awaga, *Angew. Chem., Int. Ed.*, 2011, **50**, 3471; (*g*) H. Tanaka, M. Akai-Kasaya, A. TermehYousefi, L. Hong, L. Fu, H. Tamukoh, D. Tanaka, T. Asai and T. Ogawa, *Nat. Commun.*, 2018, **9**, 2693; (*h*) Y.-R. Wang, Q. Huang, C.-T. He, Y. Chen, J. Liu, F.-C. Shen and Y.-Q. Lan, *Nat. Commun.*, 2018, **9**, 4466.

9 (*a*) L. Pettersson, I. Andersson and L.-O. Öhman, *Acta Chem. Scand., Ser. A*, 1985, **39**, 53; (*b*) L. Pettersson, I. Andersson and L.-O. Öhman, *Inorg. Chem.*, 1986, **25**, 4726; (*c*) L. Pettersson, *Acta Chem. Scand., Ser. A*, 1975, **29**, 677; (*d*) G. Johansson, L. Pettersson and N. Ingri, *Acta Chem. Scand., Ser. A*, 1978, **32**, 681; (*e*) O. W. Howarth, L. Petterson and I. Andersson, *J. Chem. Soc., Dalton Trans.*, 1991, 1799.

10 (*a*) J. Bulis, D. Garay-Ruiz, M. Segado-Centallas, E. Petrus and C. Bo, *Chem. Sci.*, 2024, **15**, 14218; (*b*) J. Build, D. Garay-Ruiz, E. Petrus, M. Segado-Centallas and C. Bo, *ChemRxiv*, 2024, preprint, DOI:DOI: **10.26434/chemrxiv-2024-r2lsq**.

11 S. Himeno, M. Hashimoto and T. Ueda, *Inorg. Chim. Acta*, 1999, **284**, 237.

12 (*a*) A. Dolbecq, E. Dumas, C. R. Mayer and P. Mialane, *Chem. Rev.*, 2010, **110**, 6009; (*b*) J. A. R. van Veen, O. Sudmeijer, C. A. Emeis and H. de Wit, *J. Chem. Soc., Dalton Trans.*, 1986, 1825; (*c*) L. Pettersson, I. Andersson and L.-O. Öhman, *Inorg. Chem.*, 1986, **25**, 4726; (*d*) C. Marchal-Roch, E. Ayrault, L. Lisnard, J. Marrot, F.-X. Liu and F. Sécheresse, *J. Cluster Sci.*, 2006, **17**, 283; (*e*) F. Li and L. Xu, *Dalton Trans.*, 2011, **40**, 4024.

13 C. Li, N. Mizuno, K. Yamaguchi and K. Suzuki, *J. Am. Chem. Soc.*, 2019, **141**, 7687.

14 (*a*) C. Li, A. Jimbo, K. Yamaguchi and K. Suzuki, *Chem. Sci.*, 2021, **12**, 1240; (*b*) C. Li, K. Yamaguchi and K. Suzuki, *Chem. Commun.*, 2021, **57**, 7882.
15 (*a*) C. Li, K. Yamaguchi and K. Suzuki, *Angew. Chem., Int. Ed.*, 2021, **60**, 6960; (*b*) A. Jimbo, C. Li, K. Yonesato, T. Ushiyama, K. Yamaguchi and K. Suzuki, *Chem. Sci.*, 2023, **14**, 10280; (*c*) H. Sun, A. Jimbo, C. Li, K. Yonesato, K. Yamaguchi and K. Suzuki, *Chem. Sci.*, 2024, **15**, 9281.
16 L. A. Combs-Walker and C. L. Hill, *Inorg. Chem.*, 1991, **30**, 4016.
17 I. Kaljurand, A. Kütt, L. Sooväli, T. Rodima, V. Mäemets, I. Leito and I. A. Koppel, *J. Org. Chem.*, 2005, **70**, 1019.
18 D. Augustin-Nowacka and L. Chmurzyński, *Anal. Chim. Acta*, 1999, **381**, 215.
19 D. Qu, X. Liu, F. Duan, R. Xue, B. Li and L. Wu, *Dalton Trans.*, 2020, **49**, 12950.